

# Strong Tunneling in Double-Island Structures

Teemu Pohjola<sup>1,2</sup>, Jürgen König<sup>2</sup>, Herbert Schoeller<sup>2</sup>, and Gerd Schön<sup>1,2</sup>

<sup>1</sup>Materials Physics Laboratory, Helsinki University of Technology, 02015 HUT, Finland

<sup>2</sup>Institut für Theoretische Festkörperphysik, Universität Karlsruhe, 76128 Karlsruhe, Germany

(May 11, 2018)

We study the electron transport through a system of two low-capacitance metal islands connected in series between two electrodes. The work is motivated in part by experiments on semiconducting double-dots, which show intriguing effects arising from coherent tunneling of electrons and mixing of the single-electron states across tunneling barriers. In this article, we show how coherent tunneling affects metallic systems and leads to a mixing of the *macroscopic* charge states across the barriers. We apply a recently formulated RG approach to examine the linear response of the system with high tunnel conductances (up to  $8e^2/h$ ). In addition we calculate the (second order) cotunneling contributions to the non-linear conductance. Our main results are that the peaks in the linear and nonlinear conductance as a function of the gate voltage are reduced and broadened in an asymmetric way, as well as shifted in their positions. In the limit where the two islands are coupled weakly to the electrodes, we compare to theoretical results obtained by Golden and Halperin and Matveev *et al.*. In the opposite case when the two islands are coupled more strongly to the leads than to each other, the peaks are found to shift, in qualitative agreement with the recent prediction of Andrei *et al.* for a similar double-dot system which exhibits a phase transition.

73.23.-b, 73.23.Hk, 73.40.Rw

## I. INTRODUCTION

Electron transport through small metal islands displays single-electron effects such as Coulomb-blockade and gate-voltage dependent oscillations of the conductance<sup>1–4</sup>. Most of these effects can be explained in terms of lowest-order perturbation theory<sup>1</sup>, but recently it has been found – in experiment and theory – that in several regimes higher-order tunneling processes need to be taken into account. These are the Coulomb-blockade regime, where sequential tunneling is exponentially suppressed, and the regime close to resonances. In the former the dominant contribution to the current is due to cotunneling processes, where electrons tunnel through the system via virtual intermediate states<sup>5,6</sup>. Close to the resonances, cotunneling and higher-order processes can significantly affect the linear and nonlinear conductance even though the lowest-order processes are *not* suppressed<sup>6–9</sup>.

In this work we study equilibrium and non-equilibrium electron transport through the double-island system

shown in Fig. 1. Structures consisting of two coupled metal islands or large quantum dots (large enough to blur the discreteness of energy levels) have recently received considerable attention<sup>10–16</sup>. The present work differs from the previous ones in two major respects. Firstly, in Refs. 10–14 and 16 dots have been investigated which are coupled by just one or a few conducting channels, while in the present work a large number  $N$  of parallel channels in each junction is considered<sup>17</sup>. (Ref. 15 also discusses how an arbitrary number of channels in the middle junction affects the positions of the conductance peaks.) Secondly, previous work has concentrated on two limiting cases: either strong tunneling between the two islands or between the islands and the leads, while we allow for arbitrary relations between the various junction conductances.

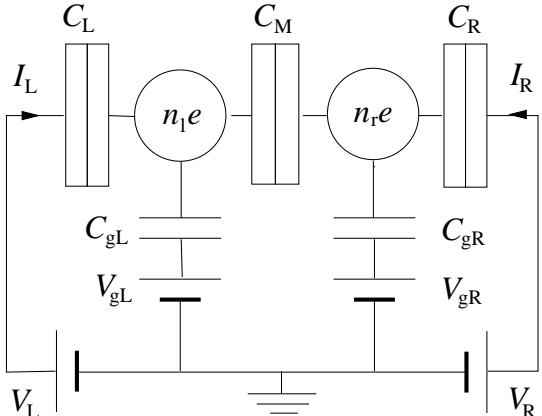


FIG. 1. A schematic picture of a double-island structure with the voltage sources and various capacities in the system. The two circles denote the islands with  $n_l/n_r$  excess electrons.

Systems of tunnel junctions are described by two characteristic quantities. The first is the charging energy for a given charge configuration  $(n_l, n_r)$  on the islands,

$$E_{\text{ch}}(n_l, n_r) = E_{\text{CL}}(n_l - n_{x,1})^2 + E_{\text{CR}}(n_r - n_{x,r})^2 + E_{\text{CM}}(n_l - n_{x,1})(n_r - n_{x,r}). \quad (1)$$

It is displayed in Fig. 2 for the four lowest states. The coefficients  $E_{Cb}$ , with  $b = L, M, R$ , are the appropriate capacitive energy scales, which in general depend on all capacitances. The gate charges  $n_{x,1} = V_{gL}C_{gL}/e + V_L C_L/e$  and  $n_{x,r} = V_{gR}C_{gR}/e + V_R C_R/e$  control the charge on the islands, see Fig. 3. For convenience, we consider below a left-right symmetric situation:  $C_L = C_R = C$ ,  $C_{gL} = C_{gR} = C_g$ , and  $n_{x,1} = n_{x,r} = n_x$ . The charging energy contains two energy scales. One,

$$E_C = \frac{e^2}{2} \frac{1}{2(C + C_g)}$$

depends on the external capacitances and determines the curvature of the parabolas. The other scale,

$$E_{CM} = \frac{e^2}{2} \frac{2C_M}{(C + C_g)(C + 2C_M + C_g)},$$

also depends on the capacitive coupling,  $C_M$ , of the two islands and leads to a splitting as displayed in Fig. 2. The other important set of parameters are the dimensionless tunneling conductances through the junctions  $b$

$$\alpha_0^b = \frac{1}{4\pi^2} \frac{h}{e^2 R_{T,b}}. \quad (2)$$

Also here we choose left-right symmetry,  $\alpha_0^L = \alpha_0^R$ , but do not fix the ratio between  $\alpha_0^M$  and  $\alpha_0^{L,R}$ .

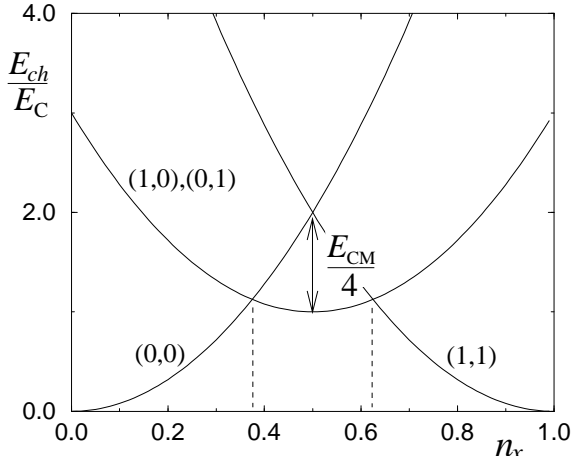


FIG. 2. Charging energy of the four lowest-lying states for the case of equal gate charges  $n_x = n_{xL} = n_{xr}$ . The states are denoted by  $(0,0)$ ,  $(1,0)$ ,  $(0,1)$ , and  $(1,1)$ . At temperatures  $T \ll E_{CM}/4$ , electron transport takes place in the regions around the degeneracy points of energy, depicted in the figure by the vertical dashed lines.

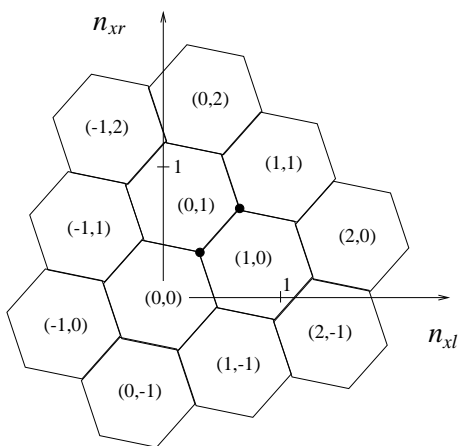


FIG. 3. The honeycomb in the  $(n_{xL}, n_{xr})$ -plane shows the regions where a given state  $(n_x, n_r)$  has the lowest energy. The circles denote the degeneracy points of Fig. 2.

In this article we study the system using two approaches. Firstly, we make use of the real-time diagrammatic technique developed for metal islands<sup>6–8</sup> and quantum dots<sup>18</sup>. This approach is applicable for linear and nonlinear response and all values of the gate voltages. In the main text, we discuss a systematic perturbative expansion of the diagrams and, in appendix A, present the calculation done up to second-order in the tunneling conductances. This calculation accounts for all second-order tunneling processes and turns out to be independent of any cutoffs. Secondly, in order to consider stronger tunneling, we study the double-island system in terms of a recently-developed renormalization-group approach<sup>19</sup>. In its general form, this procedure is cutoff independent and allows us to include all charge states. It thus differs from the RG approach developed in Ref. 20, which only uses two adjacent charge states of the single-electron box and which requires a cutoff of the order of the charging energy  $E_C$ . We apply the RG equations in their equilibrium form, which is sufficient for the linear conductance close to resonances, and consider tunneling conductances up to  $8e^2/h$  ( $\alpha_0^b$ 's up to 0.20).

Our main results are the following. In the weak-tunneling limit,  $\alpha_0^b \ll 1$ , and low temperature  $T \ll E_{CM}/4$  the linear conductance  $G$  displays a series of peaks as a function of the gate voltage. As the tunneling conductances  $\alpha_0^b$  are increased, the peak heights are reduced with a temperature dependence resembling the functional form  $1/[A + B \log(T/E_C)]$  ( $A$  and  $B$  are  $T$ -independent parameters). Also the peak positions are renormalized due to higher-order processes. For the special case when the two islands are only weakly coupled to the leads, i.e.,  $\alpha_0^M \gg \alpha_0^{L,R}$ , we reproduce the  $\alpha_0^M$ -dependences of the peak positions found in Refs. 12 and 15. As new features we find the corrections arising due to  $\alpha_0^{L,R}$  including a weak temperature dependence of the peak positions. In the opposite limit,  $\alpha_0^{L,R} \gg \alpha_0^M$  and just one channel in each junction, Andrei *et al.*<sup>16</sup> predict a phase transition: the two conductance peaks around  $n_x = 0.5$  coalesce into one as  $E_{CM}$  is reduced below a finite critical value  $E_{CM}^{\text{cr}}$ . By putting  $\alpha_0^M \ll \alpha_0^{L,R}$  we observe a similar trend for our junctions with large number of channels  $N$ .

For completeness, we use the diagrammatic technique to account for the nonlinear conductance ( $dI/dV$  at  $V \neq 0$ ) and the inelastic cotunneling processes, which cannot be studied with the equilibrium RG procedure. The nonlinear conductance displays a double-peak structure resembling that found for SET's; in the present case the peaks are typically asymmetric. Second-order processes enhance this asymmetry and pull the two peaks further apart. On top of this, the inelastic cotunneling processes result in algebraically decaying tails of the peaks both in linear and nonlinear conductance.

## II. MICROSCOPIC MODEL AND SEQUENTIAL TUNNELING

The double-island system is described by the Hamiltonian

$$\mathcal{H} = \mathcal{H}_0 + \mathcal{H}_T \quad \text{with} \\ \mathcal{H}_0 = \mathcal{H}_L + \mathcal{H}_R + \mathcal{H}_I + \mathcal{H}_r + \mathcal{H}_{ch}. \quad (3)$$

The terms  $\mathcal{H}_j$  describe noninteracting electrons in the leads and islands:  $\mathcal{H}_j = \sum_{k,n} \varepsilon_{kn}^j a_{jkn}^\dagger a_{jkn}$  with  $j \in \{L, R\}$  and  $\mathcal{H}_i = \sum_{q,n} \varepsilon_{qn}^i c_{iqn}^\dagger c_{iqn}$  with  $i \in \{l, r\}$ . The indices  $k$  and  $q$  label the electronic states, and  $n = 1 \dots N$  labels the transverse channels. We assume that the number of channels  $N$  in each junctions is large. The Coulomb interactions are described by the term  $\mathcal{H}_{ch}$  which is the operator form of Eq. (1). Tunneling of electrons is described in terms of the tunneling Hamiltonian

$$\mathcal{H}_T = \sum_{kqn} \left( T_{kq}^{Ln} a_{Lkn}^\dagger c_{lqn} e^{-i\hat{\phi}_l} + \text{H.c.} \right) \\ + \sum_{kqn} \left( T_{kq}^{Rn} a_{Rkn}^\dagger c_{rqn} e^{-i\hat{\phi}_r} + \text{H.c.} \right) \\ + \sum_{qq'n} \left( T_{qq'}^{Mn} c_{lqn}^\dagger c_{r'qn} e^{i(\hat{\phi}_l - \hat{\phi}_r)} + \text{H.c.} \right), \quad (4)$$

where  $T_{kq}^{bn}$  are the tunneling matrix elements for the barriers  $b$  (below we assume  $T_{kq}^{bn} = T^{bn}$ ). They are related to the tunneling resistances, e.g., for the right junction via

$$\alpha_0^R = \frac{1}{4\pi^2} \frac{h}{e^2 R_{T,R}} = \sum_n N_R(0) N_r(0) |T^{R,n}|^2. \quad (5)$$

Here  $N_{R/r}(0)$  is the density of states in the right lead/island and the operator  $e^{\pm i\hat{\phi}_i}$  changes the charge on the island  $i$  by  $\pm e$ .

Due to the periodicity of energies, it is sufficient to concentrate on gate voltages in the range  $0 \leq n_x \leq 0.5$ . In this interval, the tunneling of electrons through the barrier  $b = L, M, R$  is characterized by the following differences in charging energies:  $\Delta_L \equiv E_{ch}(1,0) - E_{ch}(0,0)$ ,  $\Delta_R \equiv E_{ch}(0,1) - E_{ch}(0,0)$ , and  $\Delta_M \equiv E_{ch}(0,1) - E_{ch}(1,0)$ .

In the weak tunneling limit,  $\alpha_0 \ll 1$ , sequential tunneling processes dominate. At low temperatures only the states  $(0,0)$ ,  $(1,0)$ , and  $(0,1)$  participate in the transport and we obtain the following expression for the current

$$I^{\text{seq}} = \frac{2\pi e}{\hbar} \times \frac{\alpha_L \alpha_M \alpha_R (f_L^+ f_M^+ f_R^- - f_L^- f_M^- f_R^+)}{\alpha_M^+ \alpha_R + \alpha_M^- \alpha_L + \alpha_M^+ \alpha_L^+ + \alpha_M^- \alpha_R^+ + \alpha_R^- \alpha_L + \alpha_R^+ \alpha_L^-}. \quad (6)$$

For compactness of this expression, we have omitted the argument  $\Delta_b$  from both the sequential-tunneling rates

$$\alpha_b^\pm(\Delta_b) = \pm \alpha_0^b \frac{\Delta_b - \Delta\mu_b}{\exp[\pm\beta(\Delta_b - \Delta\mu_b)] - 1} \quad (7)$$

for the barriers  $b$  as well as the Fermi functions  $f_b^\pm(\Delta_b) = (\exp[\pm\beta(\Delta_b - \Delta\mu_b)] + 1)^{-1}$  ( $\Delta\mu_b$  is the difference in chemical potentials across barrier  $b$ ). We further introduced  $\alpha_b \equiv \alpha_b^+(\Delta_b) + \alpha_b^-(\Delta_b)$ .

Already the sequential-tunneling current, Eq. (6), displays interesting properties not found in single-island transistors. In the linear conductance regime one would expect to find the conductance peak at the degeneracy point, and this is indeed the case when all  $\alpha_0^b$  are equal. In the asymmetric case,  $\alpha_0^M \neq \alpha_0^{L,R}$ , the peak acquires a temperature-dependent shift (vanishing at  $T = 0$ ). The direction of the shift depends on the relative magnitude of  $\alpha_0^M$  and  $\alpha_0^L = \alpha_0^R$  as shown in Fig. 4. Remarkably, the linear conductance at the degeneracy point is always given by the temperature-independent expression

$$G^* = \frac{2\pi e^2}{3\hbar} \frac{\alpha_0^L \alpha_0^M \alpha_0^R}{\alpha_0^L \alpha_0^M + \alpha_0^L \alpha_0^R + \alpha_0^M \alpha_0^R} \quad (8)$$

corresponding to the intersection point,  $n_x = 0.375$ , in Fig. 4.

In what follows, we account for charge fluctuations through all three junctions. We do this using two complementary approaches: a real-time diagrammatic technique and a renormalization-group analysis.

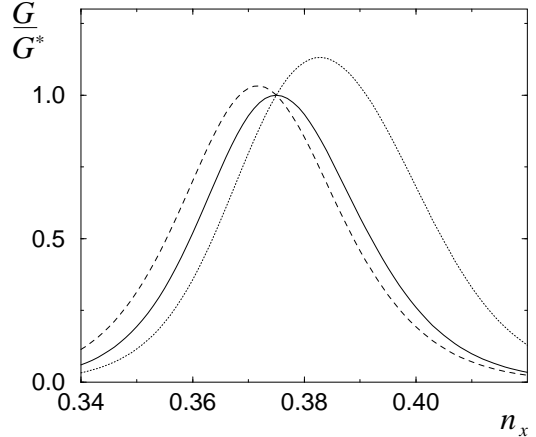


FIG. 4. Sequential-tunneling conductance for junction conductances  $\alpha_0^M = \alpha_0^{L,R} = 0.01$  (solid line),  $\alpha_0^M = 0.001$ ,  $\alpha_0^{L,R} = 0.01$  (dotted line), and  $\alpha_0^M = 0.01$ ,  $\alpha_0^{L,R} = 0.001$  (dashed line). The curves intersect at the degeneracy point of the charging energies due to scaling with Eq. (8). For  $\alpha_0^M$  larger (smaller) than  $\alpha_0^{L,R}$  increasing temperature shifts the peak to the left (right).

### III. DIAGRAMMATIC APPROACH

The physical properties, including the nonequilibrium dynamics of the double-island system, are described by a reduced density matrix. We study the time evolution of this density matrix in a basis of charge states,  $\chi = (n_{l,\chi}, n_{r,\chi})$ , and perform an expansion in  $\mathcal{H}_T$ . This leads to a formally exact master equation for the occupation probabilities  $p_\chi$  in terms of general transition rates  $\Sigma_{\chi,\chi'}$  which remain to be evaluated. In the stationary limit the master equation reads<sup>7,8</sup>

$$0 = \dot{p}_\chi = \sum_{\chi' \neq \chi} [p_{\chi'} \Sigma_{\chi',\chi} - p_\chi \Sigma_{\chi,\chi'}]. \quad (9)$$

Also the stationary current through the junction  $b$  can be expressed in terms of rates and probabilities,

$$\langle I_b \rangle = -ie \sum_{\chi,\chi'} p_{\chi'} \Sigma_{\chi',\chi}^{b+}. \quad (10)$$

The rate  $\Sigma_{\chi',\chi}^{b+}$  with the plus sign is a subset of all possible rates contained in  $\Sigma_{\chi,\chi'}$ <sup>21</sup>. We refer the reader to Refs. 4 and 18 for a more thorough discussion on the above equation.

The nonequilibrium time evolution of the density matrix may be visualized in terms of diagrams. In particular, the rate  $\Sigma_{\chi,\chi'}$  is a sum of all possible processes of which Fig. 5 shows some examples. In previous work, two approaches have been used for evaluating the rates. In the so-called resonant-tunneling approximation<sup>7,8</sup> one accounts for an infinite sum of terms of a certain form via the use of self-consistent equations in the spirit of the Dyson equation. This approach accounts for high-order tunneling processes but is, in practice, limited to a small number of charge states. In the alternative, a systematic perturbative expansion of the diagrams<sup>6</sup>, one includes all processes of a given order  $O(\alpha_0^k)$ . The key advantage of this approach is that, for not too high tunneling conductances, it can account for a larger number of charge states.

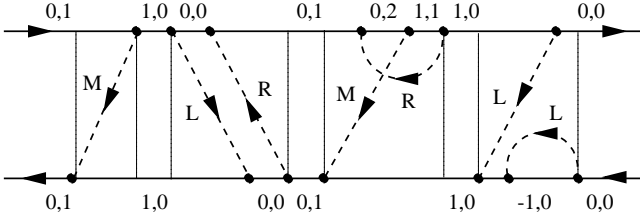


FIG. 5. Example of the diagrammatic representation of the time evolution of the reduced density matrix. In the diagrams one can distinguish different tunneling processes (the vertical dotted lines are meant to guide the eye), from left to right, sequential tunneling, inelastic cotunneling, and second-order processes leading to vertex and propagator corrections. The pairs of numbers on the forward and backward propagators (the horizontal lines) correspond to charge states, the dashed lines with labels  $b$  describe tunneling of electrons across junction  $b$ .

The probabilities and rates can be expanded in powers of  $\alpha_0$ <sup>18,6</sup>

$$p_\chi = p_\chi^{(0)} + p_\chi^{(1)} + p_\chi^{(2)} + \dots$$

$$\Sigma_{\chi,\chi'} = \Sigma_{\chi,\chi'}^{(1)} + \Sigma_{\chi,\chi'}^{(2)} + \Sigma_{\chi,\chi'}^{(3)} + \dots, \quad (11)$$

where  $p_\chi^{(k)}$  and  $\Sigma_{\chi,\chi'}^{(k)}$  denote the terms  $\sim \alpha_0^k$ . Figure 5 exemplifies processes contributing to the rates  $\Sigma^{(k)}$  with  $k = 1, 2$ . When the expressions (11) are inserted into the master equation, Eq. (9), this must hold in each order and once we know the rates we may iteratively solve for  $p^{(k)}$ . The probabilities and rates together determine the average charge on the islands  $\langle n_i \rangle = \sum_\chi n_{i,\chi} p_{i,\chi}$  as well as the current  $I \equiv \langle I_b \rangle$ , from Eq. (10).

A second-order calculation ( $O(\alpha_0^2)$ ) that accounts for all charge states (reachable in this order) has proven its virtues in the study of SET's: the calculations could be carried out exactly and all cutoff dependences vanish from the physical quantities. Also the comparison<sup>6</sup> with experiments showed that proper consideration of cotunneling processes gives correct results for a wide range of tunneling conductances and also at resonances. A similar second-order calculation for the double-island system together with rules for evaluating the individual diagrams is presented in appendix A. Also the results for linear and nonlinear conductance are shown there.

### IV. RENORMALIZATION GROUP ANALYSIS

In the strong tunneling regime, such as attained in recent experiments on single-electron transistors<sup>9</sup>, it is necessary to go beyond low-order expansions in the tunneling conductances. To this end, we study the double-island system using a recently developed real-time RG procedure<sup>19</sup>. In its general form, this procedure accounts for an arbitrary number of charge states and is independent of any cutoffs. Below we use the equilibrium form of the RG equations which yields the renormalization of system parameters. We extend the equilibrium description of the system to account for transport properties via the following assumption: for not too large  $\alpha_0^b$  the linear conductance is given up to small regular terms by the sequential-tunneling expressions when we replace all the bare parameters with the renormalized ones. The linear conductance obtained in this manner is consistent with the diagrammatic calculation at least up to  $O(\alpha_0^2)$ . It should be noted that this approach does not account for the inelastic cotunneling processes. However, here we are mainly interested in the region around the conductance maximum where, at least in the order  $O(\alpha_0^2)$ , these only result in a weak temperature independent correction (similar result obtained for a SET).

The results from the full RG are obtained numerically and are thus presented graphically. For small  $\alpha_0^b$  the RG flow equations can be expanded analytically

up to  $O(\alpha_0^2)$  and we can complement the numerical results with the analytical formulas obtained in this order. The energy differences  $\Delta^{(0)}(n_x) = E_{\text{ch}}(1,0;n_x) - E_{\text{ch}}(0,0;n_x) = E_{\text{ch}}(0,1;n_x) - E_{\text{ch}}(0,0;n_x)$  and the tunneling conductances  $\alpha_0^b$  are found to be renormalized to  $\tilde{\Delta}(n_x) = \Delta^{(0)}(n_x) + \Delta^{(1)}(n_x)$  and  $\tilde{\alpha}^b = \alpha_0^b + \alpha_b^{(2)}$ , respectively. The former yields directly the renormalized degeneracy point,  $n_x^*$ , following from the condition  $\tilde{\Delta}(n_x^*) = \Delta^{(0)}(n_x^*) + \Delta^{(1)}(n_x^*) = 0$ , see Ref. 22. One should keep in mind that the peak arising from the expression for the sequential-tunneling conductance is not necessarily located at the degeneracy point, see Fig. 4. The peak may be shifted due to unequal  $\alpha_0^b$  but also for large  $\alpha_0^b$  because these can become significantly unequal in the renormalization flow. The full RG equations as well as their  $O(\alpha_0^2)$ -expansion (see below) for the general case are sketched in Appendix B.

## V. RESULTS

Figure 6 shows the main effects of increasing tunneling strength on the linear conductance: the conductance peak is shifted and broadened and its maximum is reduced. Furthermore the peak shape, in particular in the tail regions, becomes asymmetric. The key for understanding the changes around the conductance peak maximum is the renormalization of the system parameters: the peak lies at or close to the position of the degeneracy point, see Fig. 2, which is determined by the capacitive energies  $\tilde{E}_C$  and  $\tilde{E}_{CM}$ , the peak width depends on the curvature of the energy parabolas,  $\tilde{E}_C$ , and the peak height on the tunneling conductances  $\tilde{\alpha}_b$ . For increasing tunneling strength, the effective capacitances  $\tilde{C}_b$  typically increase (modifying  $E_{Cb}$  into  $\tilde{E}_{Cb}$ ) while  $\tilde{\alpha}_b$  decrease. The fluctuations through the middle and the outer junctions affect the system in qualitatively different manner and below we distinguish between the three cases,  $\alpha_0^M \gg \alpha_0^{L,R}$ ,  $\alpha_0^M \ll \alpha_0^{L,R}$  and  $\alpha_0^M = \alpha_0^{L,R}$ . In all the figures, we have chosen left-right symmetry and, unless otherwise mentioned, used the convention  $C_L = C_R = C_M = 100C_{gL} = 100C_{gR}$  similar to the experimental values of Joyez *et al.*<sup>9</sup>. In terms of the charging energies, this corresponds to  $E_{CM} \approx E_{CL,R} \approx \frac{4}{3}E_C$ .

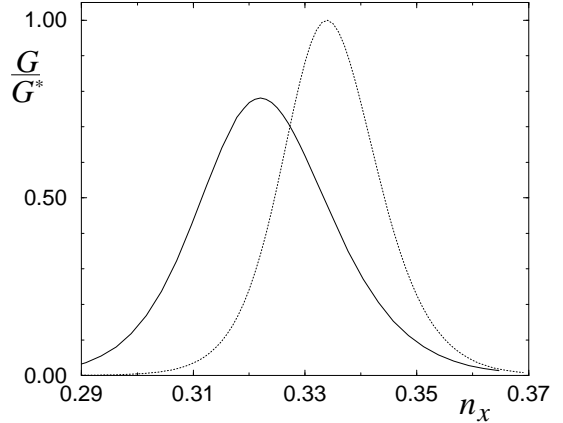


FIG. 6. The solid line shows an example of the linear conductance peak as obtained with the full RG calculation. The dotted curve is the sequential-tunneling conductance for the same parameters. Here  $\alpha_0^L = \alpha_0^R = 0.025$ ,  $\alpha_0^M = 0.05$  and  $\ln(T/E_C) = -4$ .

The case  $\alpha_0^M \gg \alpha_0^{L,R}$  consists of a subsystem, the two islands, whose properties are probed via the weak tunneling junctions connecting the subsystem to the leads. For weak coupling between the islands, i.e., small  $\alpha_0^M$ , the electrons in each island form well-defined quantum states. For increasing  $\alpha_0^M$ , the states in different islands become increasingly mixed reducing the resulting ground-state energy. In terms of the system parameters, this can be seen as an increase in  $C_M$  – increase in  $E_{CM}$  – which lowers the energy of the states  $(1,0)$  and  $(0,1)$  and shifts  $n_x^*$  correspondingly, see Figs. 7 and 2. The renormalization of  $\alpha_0^b$ 's and  $\Delta$  is independent of the gate voltage and the peak width remains given by thermal broadening.

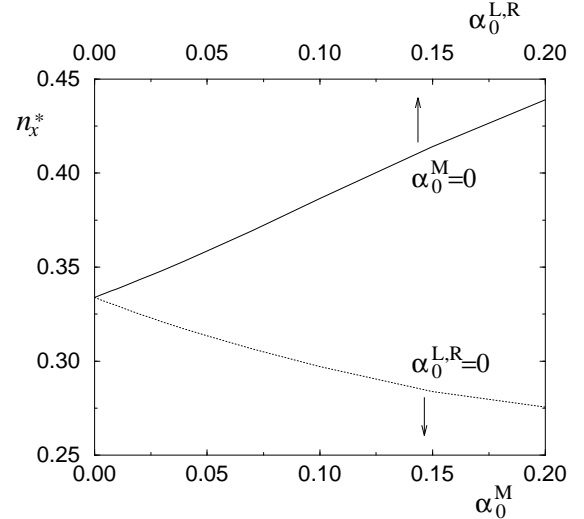


FIG. 7. The position of the degeneracy point  $n_x^*$  at  $T = 0$  as a function of  $\alpha_0^M$  with  $\alpha_0^{L,R} = 0$  (dotted line, lower horizontal axis) and  $\alpha_0^{L,R} \neq 0$  (solid line, upper horizontal axis).

Figure 8 displays the temperature dependence of the maximum conductance (the curves approach logarithmic form for  $\alpha_0^M \rightarrow 0$ ). It shows also the maximum conductance for  $\alpha_0^M = 0.01$  as obtained in second-order. The functional form is seen to differ from the corresponding RG result in three ways. First, the overall diverging shape is due to an unphysical  $\Delta^{(1)}/T$ -dependence of the perturbation expansion, emphasized for cases where the peak experiences a strong shift (large  $\Delta^{(1)}$ ). Second, the initial slope at higher temperatures is slightly overestimated by the second-order result. Third, the maximum conductance is shifted downwards as compared to the RG result. This is due to the neglect of the inelastic cotunneling contributions in the RG calculation.

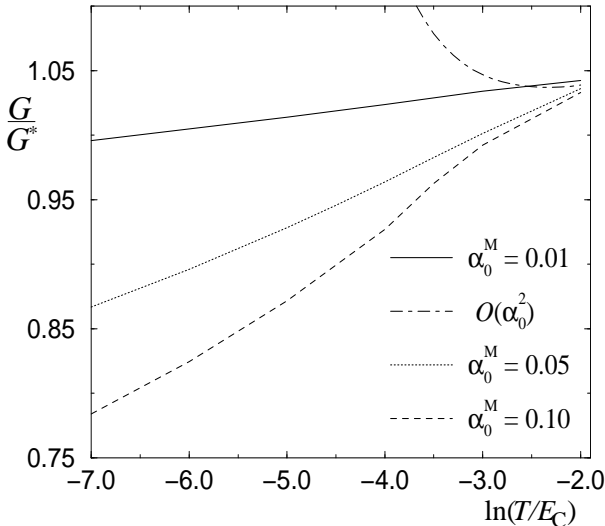


FIG. 8. Temperature dependence of the conductance maxima for  $\alpha_0^M = 0.01, 0.05, 0.1$ . The curves approach logarithmic form for  $\alpha_0^M \rightarrow 0$ . The upward shooting curve is the second-order result for  $\alpha_0^M = 0.01$ , see text for further discussion on its shape.

The limit  $\alpha_0^{L,R} \gg \alpha_0^M$  corresponds to two interconnected single-electron boxes (SEB) where the small conductance at the central junction can be used to probe the capacitive interactions of the two systems. Similar to single SEB's, increasing tunneling conductance in the junction  $b$  increases the capacitance  $C_b$  resulting in reduced curvature of the energy parabolas and smaller  $\tilde{\Delta}$ 's. This can be seen as a broadening and shifting of the conductance peaks. The resulting peak shift is shown in Fig. 7 as a function of  $\alpha_0^{L,R}$ . Increasing tunneling conductance also results in a gate-voltage and temperature dependent renormalization of  $\tilde{\alpha}_{L,R}$  and  $\tilde{\alpha}_M$  reducing these quantities. Figure 9 shows the full conductance curves for two choices of  $\alpha_0^{L,R}$ . The curious shape of the peaks is a consequence of the interplay of two effects: at a finite temperature the peak is shifted away from  $n_x^*$  due to unequal  $\alpha_0^b$ 's, see above, while  $\tilde{\alpha}_b$  reduce the conductance around  $n_x^*$ , i.e., not quite at the actual maximum.

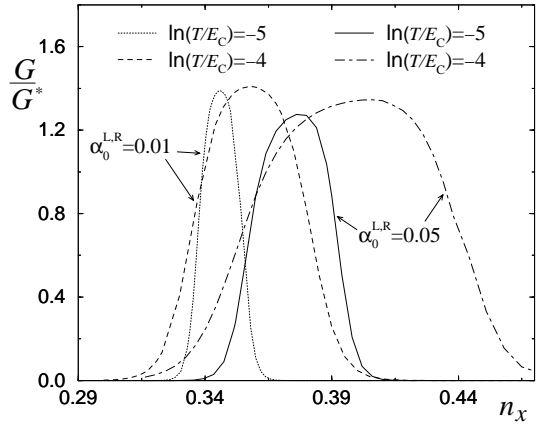


FIG. 9. The full conductance curve at  $\ln(T/E_C) = -5, -4$  for  $\alpha_0^{L,R} = 0.01$  (dotted and dashed, respectively) and for  $\alpha_0^{L,R} = 0.05$  (solid and dot-dashed, respectively). The degeneracy points of energy are located at 0.3385 and 0.3586 for  $\alpha_0^{L,R} = 0.01, 0.05$ , respectively.

Before going to the third case of equal  $\alpha_0^b$ 's, let us write down the main results obtained by expanding the RG equations to  $O(\alpha_0^2)$  and make comparison to results in the literature. The renormalized degeneracy point,  $n_x^*$ , follows from the condition  $\tilde{\Delta}(n_x^*) = \Delta^{(0)}(n_x^*) + \Delta^{(1)}(n_x^*) = 0$ . In the zero-temperature limit, the RG calculation yields the temperature- and  $n_x$ -independent correction

$$\begin{aligned} \Delta^{(1)} = & \alpha_0^L \left( 2E_{CL} \ln \left| \frac{2E_{CL}}{2E_{CL} - E_{CM}} \right| + E_{CM} \ln \left| \frac{2E_{CL} - E_{CM}}{E_{CM}} \right| \right) \\ & - \alpha_0^M (4E_{CL} - 2E_{CM}) \ln 2. \end{aligned} \quad (12)$$

For the special case  $E_{CL,R} = E_{CM}$ , the prefactors of  $\alpha_0^M$  and  $\alpha_0^L$  are equal. This linear  $\alpha_0^M$ -dependence is a new result whereas the  $\alpha_0^M$ -dependence equals the results in Refs. 14,15,12 (shown to be independent of  $N$  in Ref. 15). Further examination of the  $\alpha_0^M$ -dependent curve in Fig. 7 in terms of polynomial fitting yields the coefficient of the quadratic term within 1-2% of the analytical result Ref. 15. It should be noted that this accuracy already requires six correct decimals in calculating  $n_x^*$ . The  $\alpha_0^L$ -dependent curve in Fig. 7 remains very close to linear up to the largest  $\alpha_0^{L,R}$  used here. However, if we repeat the calculation with a smaller value of  $E_{CM}$  the curve only approaches the line  $n_x = 0.5$  asymptotically.

An expression for the temperature dependence of the peak conductance may be found by inserting the renormalized  $\alpha_0^b$ 's to Eq. (8). This corresponds to the requirement that at resonance  $\tilde{\Delta}(n_x^*) = 0$  and yields

$$\begin{aligned} G &= G^{\text{seq}} + G^{(2)} \\ &= G^{\text{seq}} \left[ 1 + \frac{B_1(\alpha_0^L)^2 + B_2\alpha_0^L\alpha_0^M + B_3(\alpha_0^M)^2}{2\alpha_0^M + \alpha_0^L} \right] \end{aligned} \quad (13)$$

with the temperature dependent parameters  $B_i$ :  $B_1 = 2 \ln |T/E_{CM}|$ ,  $B_2 = 8 \ln |T/E_{CM}|$ , and  $B_3 = \ln |T/E_{CM}|$ . For  $\alpha = \alpha_0^{L,R} = \alpha_0^M$  we obtain the limiting form

$$G^{(2)} \propto \frac{4}{9} \alpha^2 \ln |T/E_{\text{CM}}|. \quad (14)$$

In this order, this is the sole source of temperature dependence to the maximum value of  $G$ . In the more general case  $\alpha_0^{\text{L,R}} \neq \alpha_0^{\text{M}}$ , the peak is not at the point  $n_x^*$  and one should use the full form for  $G$ .

In the complete case, when charge fluctuations are allowed through all three junctions, the above-discussed effects intermingle in a complicated way. Now all the energies  $E_{\text{Cb}}$  and tunneling conductances  $\alpha_0^b$  are renormalized with some contributions to these depending on gate voltages and/or temperature while some others remain constant. In the following we consider for convenience the case of all  $\alpha_0^b$  being equal. Even in this case, the peak may be shifted, cf. Eq. (12), but, in order to see the changes in the peak shapes more easily, the capacitances are chosen such that  $n_x^*$  is independent of the tunneling conductances. The choice of capacitances adopted above is close to the special case  $E_{\text{CL,R}} = E_{\text{CM}}$  with no shift in the second order and it appears that in this case there is no shift in higher orders either. Figure 10 shows the full conductance curves for three values of  $\alpha_0 \equiv \alpha_0^b$  at two temperatures in order to distinguish between the effects arising from thermal and quantum fluctuations. The broadening of the peaks with increasing  $\alpha_0^b$  is due to the overall reduction of  $\Delta$ 's as well as the gate-voltage dependent reduction of  $\alpha_b$ . Figure 11 shows the temperature dependence of the maximum conductance for a few values of  $\alpha_0$ . At low temperatures, the curves resemble the functional form  $1/(A + B \ln(T/E_C))$ , with the coefficient  $B$  being proportional to  $\alpha_0$ . This is consistent with the assumption that the full RG calculation resums the leading logarithmic terms  $\alpha_0 \ln(T/E_C)$ . Figure 11 also shows the second-order result for  $\alpha_0 = 0.01$  with the slope given by Eq. (14). The  $\Delta^{(1)}/T$ -behaviour of Fig. 8 is absent because the peak is not shifted and  $\Delta^{(1)}(n_x^*) = 0$ .

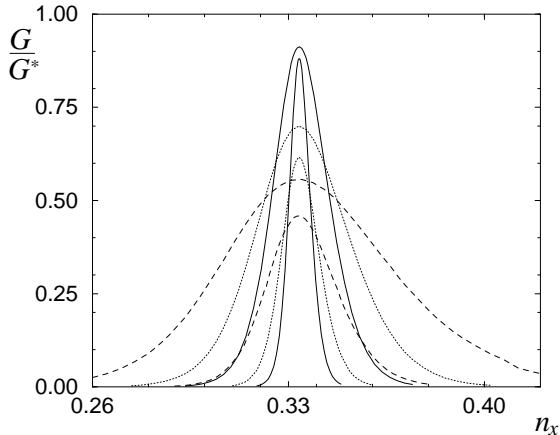


FIG. 10. The full conductance curve for  $\alpha_0 \equiv \alpha_0^{\text{L,R}} = \alpha_0^{\text{M}} = 0.01, 0.05, 0.10$  (pairs of solid, dotted and dashed curves, respectively) calculated at  $\ln(T/E_C) = -4, -5$  (upper and lower curve of each pair). The capacitances are chosen such that the peak does not shift either with temperature or with  $\alpha_0$ .

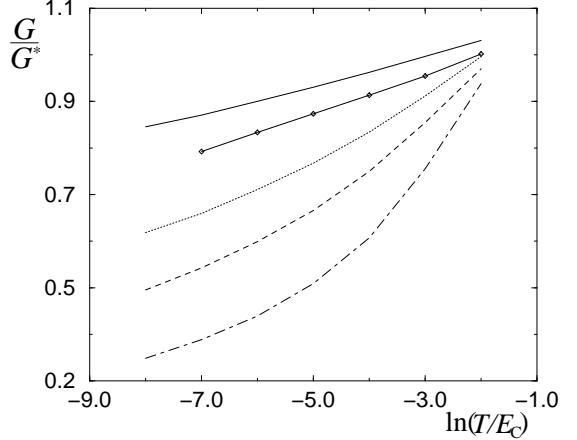


FIG. 11. Temperature dependence of the maximum conductance for  $\alpha_0 \equiv \alpha_0^{\text{L,R}} = \alpha_0^{\text{M}} = 0.01, 0.01^*, 0.03, 0.05, 0.10$  from up to down (\* the curve with the diamond symbols is the second-order result for  $\alpha_0 = 0.01$ ). Below  $\ln(T/E_C) = -3$ , the curves are of the functional form  $1/(A + B \ln(T/E_C))$ . The

## VI. CONCLUSIONS

In conclusion, we have evaluated the transport properties of a metal double-island structure using two approaches: the real-time diagrammatic technique developed in Ref. 7,8 and the RG-procedure introduced in Ref. 19. We made no *a priori* assumptions concerning the relative magnitudes of the tunneling conductances but we assumed a large number of channels in each junction. The perturbative (diagrammatic) expansion has been performed up to  $O(\alpha_0^2)$ , limiting the results to small values of  $\alpha_0$ . In this case we obtained both the linear and nonlinear response of the system for all values of gate voltage. In the RG calculation, we considered equilibrium properties of the system covering temperatures down to zero and also much larger tunnel conductances than in the perturbation theory.

Due to periodicity of the charging energies, it is sufficient to concentrate on the single conductance peak appearing in linear conductance in the gate-voltage range  $0 \leq n_x \leq 0.5$ . The height and position of this peak are found to be renormalized and its shape becomes asymmetric. In general, we do not need to restrict the relative magnitudes of the tunneling conductances  $\alpha_0^b$ , but

two limiting cases can be compared to existing work on similar systems. In the limit of  $\alpha_0^M \gg \alpha_0^L = \alpha_0^R$ , we reproduce the third-order results for the peak position reported by Golden and Halperin<sup>15</sup>. In the opposite limit,  $\alpha_0^M \ll \alpha_0^L = \alpha_0^R$ , the system resembles the model considered by Andrei *et al.*<sup>16</sup>. These authors studied the mapping of a double-island system with one conducting channel in all junctions onto a Kondo model. It was predicted that the system would undergo a phase transition as a function of  $E_{\text{CM}}$ , the mutual interaction energy for electrons in different islands: the two conductance peaks around  $n_x = e/2$  merge into one as  $E_{\text{CM}}$  is reduced below some finite critical value  $E_{\text{CM}}^{cr}$ . By putting  $\alpha_0^M$  small in our calculations for many-channel junctions, we interestingly obtain a similar trend of peaks shifting towards each other, see Fig. 7.

We suggest the following experimental schemes similar to those used in Ref. 9: one could measure the heights both the linear and nonlinear conductance, as well as the asymmetric shape of the double-peak structure in the nonlinear conductance  $G(n_x, V \neq 0)$ . The tunneling conductance of a single junction is typically fixed in metallic structures. However, if one could attach an additional gate partially on top of a junction itself, one might be able to control the number of conducting channels instead of the conductance of separate channels. This would enable the study of the peak position as a function of the tunneling conductances  $\alpha_0^b$ .

## VII. ACKNOWLEDGEMENTS

This work has been supported by the “Deutsche Forschungsgemeinschaft” as part of “Sonderforschungsbereich 195.” One of us (GS) also gratefully acknowledges the support through an A. v. Humboldt Research Award of the Academy of Finland and one (TP) the support through a post-graduate Research Fellowship from the Finnish Academy of Science and Letters as well as support through EU TMR Network “Dynamics of Nanosstructures”.

## APPENDIX A: DIAGRAMMATIC CALCULATION TO $O(\alpha_0^2)$

In this appendix we present a perturbative calculation of the conductance through the double-island system up to the order  $O(\alpha_0^2)$ . We also summarize the rules for evaluating the second-order rates  $\Sigma_{\chi,\chi'}^{(2)}$  in the energy representation, i.e., in Fourier space.

We begin by inserting both the probabilities and the rates in their series form, Eq. (11), into the master equation Eq. (9) and to Eq. (10) for the current. We then pick up the terms of the orders  $O(\alpha_0)$  and  $O(\alpha_0^2)$ . The lowest-order contributions are of the form  $p^{(0)}\Sigma^{(1)}$ , correspond-

ing to sequential-tunneling processes, while in the second order two kinds of corrections appear. Terms such as  $p^{(0)}\Sigma^{(2)}$  correspond to two-electron tunneling processes including the “inelastic cotunneling” processes<sup>5</sup> but also processes that give rise to renormalization of system parameters. Terms of the form  $p^{(1)}\Sigma^{(1)}$  arise due to changes in the occupation probabilities in higher orders. While away from resonances the “inelastic cotunneling” yields the dominant contribution to the current, it was recently shown that close to the resonances it is crucial to consider all these second-order terms<sup>6</sup>.

The master equation, Eq. (9), must hold in each order and once we know the rates we may iteratively solve for  $p^{(k)}$ . Hence, the essential step of the perturbative calculation consists of the evaluation of the transition rates  $\Sigma^{(1)}$  and  $\Sigma^{(2)}$ . The former are just the Golden rule rates and also the latter may be evaluated analytically as was done in Ref. 6. Before going into detail in evaluating the second-order rates, we would like to comment on two technical points. First, at intermediate stages we find it convenient to introduce a cutoff procedure to ascertain convergence of integrals. Any cutoff dependence cancels from all physical quantities, but only when we consider a set of 12 charge states – for the values of gate voltage used here these are (0,0), (1,0), (0,1), (-1,0), (0,-1), (1,1), (2,0), (0,2), (-1,1), (1,-1), (-1,2), and (2,-1)<sup>23</sup>. If we would not account for the additional charge states, the resulting quantities would contain terms with linear and logarithmic cutoff dependences. Second, for convenience, we solve the resulting set of 12 master equations numerically as this requires inverting a 12-by-12 matrix.

## 1. Rates

The tunneling rates may be visualized in terms of diagrams such as shown in Fig. 5, each diagram consisting of the following parts. The contour (solid line) corresponds to a forward and backward propagator, the upper and lower lines, respectively. Each part of the propagators has a charge state  $(n_l, n_r)$  assigned to it and it carries the corresponding energy  $E_{n_l, n_r}$ . The directed dashed lines correspond to tunneling of single electrons through the junctions. These tunneling lines carry an index  $b$ , corresponding to the junction, as well as an energy  $\omega$  of the tunneling electron. The diagrams, that cannot be divided into parts by a vertical cut through them without cutting one of the tunneling lines, are denoted irreducible diagrams and they correspond to rates of individual tunneling processes. The tunneling rates between states  $\chi$  and  $\chi'$  ( $\chi = n_{l,\chi}, n_{r,\chi}$ ) are obtained by summing up the rates of all the tunneling processes starting from the state  $\chi$  and ending up in the state  $\chi'$ .

An arbitrary diagram may be evaluated as follows. 1. Each tunneling line corresponds to the expression

$$\alpha_b^\pm(\omega) = \pm \alpha_0^b \frac{\omega - \Delta\mu_b}{\exp[\pm\beta(\omega - \Delta\mu_b)] - 1}, \quad (\text{A1})$$

with the plus (minus) sign corresponding to forward (backward) direction of the line with respect to the contour. The coefficient  $\alpha_0^b$  is the dimensionless conductance of the junction  $b$ ,  $\Delta\mu_b$  is the difference in chemical potentials across the junction and  $\omega$  is the energy of the tunneling electron. 2. In order to account for all possible tunneling processes, one integrates over the energies  $\omega$  and  $\omega'$  of the two tunneling lines. 3. The vertices, i.e., the end points of the tunneling lines, lying on the backward (lower) propagator acquire an extra factor  $-1$  each. 4. The diagrams can be divided into three parts  $i$  such that within each of them the energies of the propagators and tunneling lines remain constant. Each part  $i$  yields an energy denominator  $1/(\Delta E_i + i0^+)$  corresponding to the energy of the intermediate virtual state:  $\Delta E_i$  equals the difference of all energies of the lines (propagators and tunneling lines) directed to the left and those directed to the right. The rate of a given process is the imaginary part of the expression obtained by evaluating the corresponding diagram. For example, we obtain for the third diagram in Fig. 5

$$-i \cdot \text{Im} \cdot \int d\omega' \alpha_M^-(\omega') \int d\omega \alpha_R^+(\omega) \cdot \frac{1}{\omega' + \Delta E_1 + i0^+} \cdot \frac{1}{\omega + \omega' + \Delta E_2 + i0^+} \cdot \frac{1}{\omega + \Delta E_3 + i0^+}. \quad (\text{A2})$$

These integrals may be evaluated analytically along the lines of Ref. 6. It should be noted, that the use of these rules implicitly assumes a large number  $N$  of transverse channels in each tunnel junction.

## 2. Results

Conductance away from the peak is mainly given by the inelastic cotunneling processes and cannot be described by equilibrium calculations such as the RG analysis in the main text. For certain values of the gate voltages, the lowest energy state is doubly degenerate, see Fig. 3. In these regions we obtain a finite second-order contribution as, e.g., on the right-hand side of the peak in Fig. 12. The simplest processes that carry current through the whole double-island system are of the order  $O(\alpha_0^3)$  and hence beyond the present considerations. For this reason we only obtain the exponential decay on the left side of the peak in Fig. 12. Comparison between the present result and the RG calculation displays good agreement for small tunneling conductances thus supporting the assumption made (in RG) for the functional form of the conductance curve.

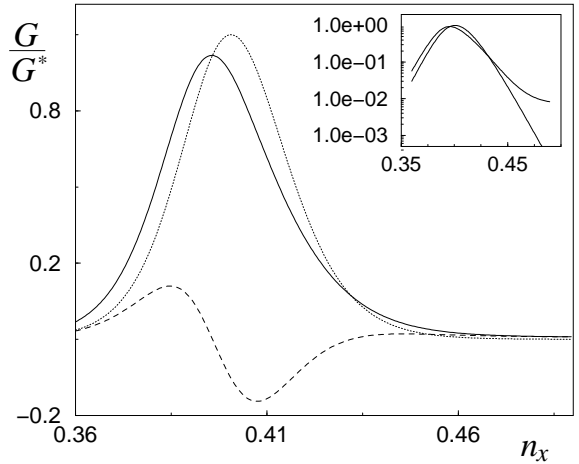


FIG. 12. Sequential tunneling (dotted), cotunneling (dashed), and the total conductance (solid) as the sum of the two as obtained from the diagrammatic calculation. The logarithmic scale in the inset emphasizes the functional difference of tails of the sequential-tunneling and total second-order conductances. The parameters used in the plots are  $\alpha_0^{\text{L,R}} = \alpha_0^M = 0.01$  and  $T = 0.03E_C$ . The junction capacitances are now chosen unequal  $C_M = \frac{1}{3}C_{\text{L,R}}$  but still two orders of magnitude larger than the gate capacitances. This results in  $E_{\text{CM}} = \frac{1}{2}E_{\text{CL,R}} = \frac{4}{5}E_C$ .

A finite transport voltage applied across the system changes the charging energies as shown in Fig. 13. At low temperature and when we only include sequential tunneling, the differential conductance  $dI/dV$  displays a double peak somewhat similar to that found in a SET but now the peaks are slightly asymmetric, see Fig. 14. For higher values of  $\alpha_0$ 's the double-peak structure may be shifted as a whole, similar to the shift of the single peak in linear conductance. In order to inspect any additional effects resulting from the finite voltage, we have chosen the parameters in Fig. 14 such that the center of the two peaks is not shifted. In this case, the peaks are shifted away from each other and the asymmetry of their heights and widths is enhanced. The different shapes of the tails are of the same origin as discussed above for the linear conductance, i.e., the asymmetric structure of the charging energies.

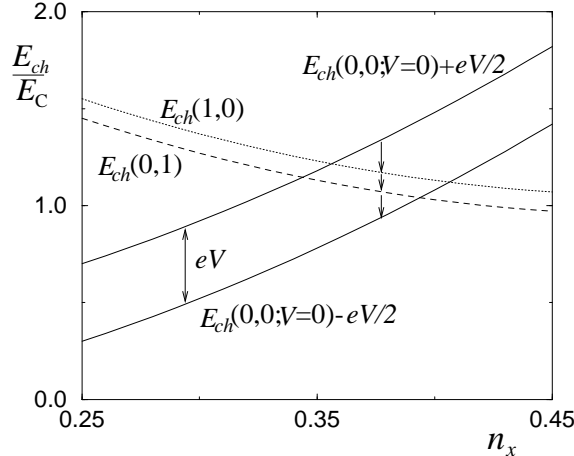


FIG. 13. Charging energy of the states  $(0,0)$ ,  $(1,0)$  and  $(0,1)$  when a finite symmetric bias voltage  $V$  is applied across the system, i.e.,  $V_L = -V_R$ . The relevant current-carrying cycle of sequential-tunneling processes is depicted with arrows.

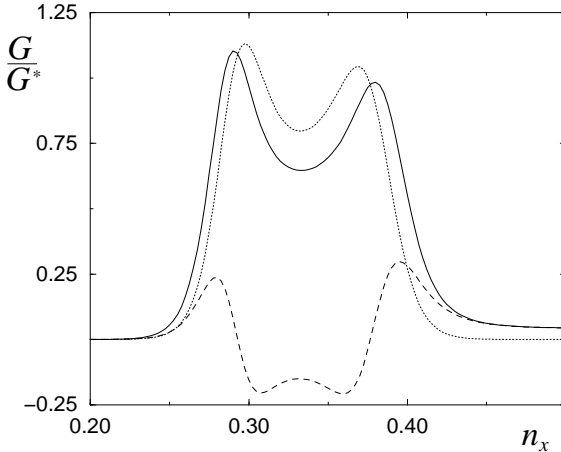


FIG. 14. Nonlinear conductance through the double-island structure: sequential tunneling (dotted) and co-tunneling (dashed) contributions, and the total conductance (solid). The peak structure is asymmetric due to the asymmetry in charging energies with respect to the peak positions. The parameters in the figure are  $eV = 0.4E_{\text{CM}}$ ,  $T = 0.03E_{\text{CM}}$ ,  $E_{\text{CM}} = E_{\text{CL,R}} = \frac{4}{3}E_C$  and all  $\alpha_0^b = 0.01$ .

## APPENDIX B: RG FORMALISM

In this Appendix we present central formulas of the RG approach applied in the second part of the text. The details may be found in<sup>19</sup>.

We study the renormalization of charging energies  $E_{n_L, n_R}$  and tunnel conductances  $\alpha_{n_L, n_R}^b$ . As the subscripts already indicate, the various  $E$ 's and  $\alpha$ 's renormalize in different ways for different charge states. For the following, let us define the differences of charging energies more generally,

$$\begin{aligned} \Delta_{n_L, n_R}^{\text{L}\sigma} &= E_{ch}(n_L + \sigma, n_R) - E_{ch}(n_L, n_R), \\ \Delta_{n_L, n_R}^{\text{R}\sigma} &= E_{ch}(n_L, n_R + \sigma) - E_{ch}(n_L, n_R), \text{ and} \\ \Delta_{n_L, n_R}^{\text{M}\sigma} &= E_{ch}(n_L, n_R + \sigma) - E_{ch}(n_L + \sigma, n_R) \end{aligned} \quad (\text{B1})$$

where  $\sigma = \pm 1$ . The quantities corresponding to those used in the diagrammatic expansion are  $\alpha_{(0,0)}^{\text{L}} = \alpha_0^{\text{L}}$ ,  $\alpha_{(0,0)}^{\text{R}} = \alpha_0^{\text{R}}$ ,  $\alpha_{(1,0)}^{\text{M}} = \alpha_0^{\text{M}}$ , and  $\Delta_{(0,0)}^{b+} = \Delta_b$ .

We study the RG flow of the charging energies directly but the tunneling conductances are obtained from the auxiliary functions  $g$  defined as

$$\begin{aligned} e^{\pm i\hat{\phi}_l} &\rightarrow \sum_{n_L, n_R} g_{n_L, n_R}^{\text{L}\pm} |n_L \pm 1, n_R\rangle \langle n_L, n_R| \\ e^{\mp i(\hat{\phi}_l - \hat{\phi}_r)} &\rightarrow \sum_{n_L, n_R} g_{n_L, n_R}^{\text{M}\pm} |n_L \pm 1, n_R \mp 1\rangle \langle n_L, n_R| \\ e^{\pm i\hat{\phi}_r} &\rightarrow \sum_{n_L, n_R} g_{n_L, n_R}^{\text{R}\pm} |n_L, n_R \pm 1\rangle \langle n_L, n_R|. \end{aligned} \quad (\text{B2})$$

These are introduced to parametrize the renormalization of  $\alpha_0$ 's

$$\begin{aligned} \alpha_{n_L, n_R}^{\text{L}} &= \alpha_0^{\text{L}} g_{n_L, n_R}^{\text{L}+} g_{n_L+1, n_R}^{\text{L}-} \\ \alpha_{n_L, n_R}^{\text{R}} &= \alpha_0^{\text{R}} g_{n_L, n_R}^{\text{R}+} g_{n_L, n_R+1}^{\text{R}-} \\ \alpha_{n_L, n_R}^{\text{M}} &= \alpha_0^{\text{M}} g_{n_L, n_R}^{\text{M}+} g_{n_L-1, n_R+1}^{\text{M}-}. \end{aligned} \quad (\text{B3})$$

Initially all  $g$ 's equal unity corresponding to the bare  $\alpha$ 's.

As an example of the full RG equations in the equilibrium case we have for the energies

$$\begin{aligned} \frac{d}{dl} \bar{\Delta}_{n_L, n_R}^{\text{L}} &= \frac{d}{dl} (\bar{E}_{n_L+1, n_R} - \bar{E}_{n_L, n_R}) = \bar{\Delta}_{n_L, n_R}^{\text{L}} \\ &+ i \sum_{\chi, \chi'} (-1)^\chi \left\{ \alpha_{n_L-\chi+\chi', n_R}^{\text{L}} \exp[-(-1)^{\chi'} i \bar{\Delta}_{n_L-\chi+\chi', n_R}^{\text{L}}] \right. \\ &- \alpha_{n_L+\chi, n_R-\chi}^{\text{R}} \exp[-(-1)^{\chi'} i \bar{\Delta}_{n_L+\chi, n_R-\chi}^{\text{R}}] \\ &\left. - \alpha_{n_L+1-\chi+\chi', n_R-\chi}^{\text{M}} \exp[-(-1)^{\chi'} i \bar{\Delta}_{n_L+1-\chi+\chi', n_R-\chi}^{\text{M}}] \right\} \end{aligned} \quad (\text{B4})$$

$$- \alpha_{n_L+1-\chi+\chi', n_R-\chi}^{\text{M}} \exp[-(-1)^{\chi'} i \bar{\Delta}_{n_L+1-\chi+\chi', n_R-\chi}^{\text{M}}] \quad (\text{B5})$$

The summation indices  $\chi$  and  $\chi'$  take values zero and one. All quantities with a bar on top of them contain the time  $t_c$  corresponding to the high-energy cutoff of the theory as, e.g.,  $\bar{E}_{n_L, n_R} = E_{n_L, n_R} t_c$ . The parameter  $l$  is defined as  $l = \ln(t_c/t_c^0)$  where  $t_c^0$  is the initial cutoff time. At the end, we take the limit  $t_c^0 \rightarrow 0$  and integrate the equations to  $t_c \rightarrow \min\{1/\Delta, 1/T\}$ .

The equations for charging energies are coupled with the flow equations for the  $g_{n_L, n_R}^{\text{b}\sigma}$ 's ( $\sigma = \pm 1$ ) which follow equations such as

$$\begin{aligned} \frac{d}{dl} g_{n_L, n_R}^{\text{L}\sigma} &= \sum_{\sigma'=\pm 1} \\ &\cdot \left\{ \alpha_0^{\text{L}} g_{n_L+\sigma-\sigma', n_R}^{\text{L}\sigma'} g_{n_L-\sigma', n_R}^{\text{L}\sigma} g_{n_L, n_R}^{\text{L}, -\sigma'} \right. \\ &\left. \frac{\exp(i \bar{\Delta}_{n_L+\sigma-\sigma', n_R}^{\text{L}\sigma'}) - \exp(i \bar{\Delta}_{n_L-\sigma', n_R}^{\text{L}\sigma'})}{i(\bar{\Delta}_{n_L+\sigma-\sigma', n_R}^{\text{L}\sigma'} - \bar{\Delta}_{n_L-\sigma', n_R}^{\text{L}\sigma'})} \right\} \end{aligned}$$

$$\begin{aligned}
& -\alpha_0^L g_{n_L, n_R}^{L\sigma} g_{n_L - \sigma', n_R}^{L\sigma'} \exp(i\bar{\Delta}_{n_L \sigma', n_R}^{L\sigma'}) \\
& + \alpha_0^R g_{n_L + \sigma, n_R - \sigma'}^{R\sigma'} g_{n_L, n_R - \sigma'}^{L\sigma} g_{n_L, n_R}^{R, -\sigma'} \\
& \quad \frac{\exp(i\bar{\Delta}_{n_L + \sigma, n_R - \sigma'}^{R\sigma'}) - \exp(i\bar{\Delta}_{n_L, n_R - \sigma'}^{R\sigma'})}{i(\bar{\Delta}_{n_L + \sigma, n_R - \sigma'}^{R\sigma'} - \bar{\Delta}_{n_L, n_R - \sigma'}^{R\sigma'})} \\
& - \alpha_0^R g_{n_L, n_R}^{L\sigma} g_{n_L, n_R - \sigma'}^{R\sigma'} g_{n_L, n_R}^{R, -\sigma'} \exp(i\bar{\Delta}_{n_L, n_R - \sigma'}^{R\sigma'}) \\
& + \alpha_0^M g_{n_L + \sigma + \sigma', n_R - \sigma'}^{M\sigma'} g_{n_L + \sigma', n_R - \sigma'}^{L\sigma} g_{n_L, n_R}^{M, -\sigma'} \\
& \quad \frac{\exp(i\bar{\Delta}_{n_L + \sigma + \sigma', n_R - \sigma'}^{M\sigma'}) - \exp(i\bar{\Delta}_{n_L + \sigma', n_R - \sigma'}^{M\sigma'})}{i(\bar{\Delta}_{n_L + \sigma + \sigma', n_R - \sigma'}^{M\sigma'} - \bar{\Delta}_{n_L + \sigma', n_R - \sigma'}^{M\sigma'})} \\
& - \alpha_0^M g_{n_L, n_R}^{L\sigma} g_{n_L + \sigma', n_R - \sigma'}^{M\sigma'} g_{n_L, n_R}^{M, -\sigma'} \exp(i\bar{\Delta}_{n_L + \sigma', n_R - \sigma'}^{M\sigma'}) \}.
\end{aligned} \tag{B6}$$

The full solution to these can be obtained via numerical integration.

Expanding the above equations up to  $O(\alpha_0^2)$  yields the leading corrections to  $\Delta$ 's and  $\alpha$ 's. The resulting equations are decoupled such that the equations for second-order quantities only depend on the respective bare quantities. For this reason the calculations can be carried out analytically. For the  $\Delta$ 's we arrive at

$$\begin{aligned}
\frac{d}{dt_c} \Delta_{n_L, n_R}^{b'(1)} = & \\
- \frac{i}{t_c^2} \sum_{b'\sigma} \alpha_0^{b'} e^{-i\Delta_{n_L, n_R}^{b'\sigma(0)} t_c} - (n_b \rightarrow n_{b+1}). &
\end{aligned} \tag{B7}$$

The notation means that the second part of the equation equals the first part up to the indicated replacements of  $n_b$ 's. Here  $b, b' \in \{L, R\}$  and  $\Delta_{n_L, n_R}^{M\sigma'} = \Delta_{n_L - \sigma', n_R}^{R\sigma'} - \Delta_{n_L - \sigma', n_R}^{L\sigma'}$ . These equations can be solved to yield

$$\begin{aligned}
\Delta_{n_L, n_R}^{b(1)}(t_c) = & +i \sum_{b'\sigma} \alpha_0^{b'} \left\{ \frac{\exp(-i\Delta_{n_L, n_R}^{L\sigma(0)} t_c)}{t_c} \right. \\
& + i\Delta_{n_L, n_R}^{L\sigma(0)} \text{Ci} \left( \left| \Delta_{n_L, n_R}^{L\sigma(0)} \right| t_c \right) + \left| \Delta_{n_L, n_R}^{L\sigma(0)} \right| \text{Si} \left( \left| \Delta_{n_L, n_R}^{L\sigma(0)} \right| t_c \right) \\
& \left. - (n_b \rightarrow n_{b+1}) \right\} - (t_c \rightarrow t_c^0) \tag{B8}
\end{aligned}$$

The functions  $\text{Ci}(x)$  and  $\text{Si}(x)$  are cosine and sine integrals.

The functions  $g^{(1)}(t_c)$  take the form as, e.g.,

$$\begin{aligned}
g_{n_L, n_R}^{b\sigma(1)}(t_c) = & \sum_{r'\sigma'} \alpha_0^{b'} \\
\cdot & \left\{ \exp(-i\Delta_{n_L, n_R}^{b'\sigma'(0)} t_c) \frac{\exp(-i\sigma\sigma' c_{rr'} t_c) - 1}{i\sigma\sigma' c_{rr'} t_c} \right. \\
+ & \left( 1 + \sigma\sigma' \frac{\Delta_{n_L, n_R}^{b'\sigma'(0)}}{c_{rr'}} \right) \\
\cdot & \left[ \text{Ci} \left( \left| \Delta_{n_L, n_R}^{b'\sigma'(0)} + \sigma\sigma' c_{bb'} \right| t_c \right) - \text{Ci} \left( \left| \Delta_{n_L, n_R}^{b'\sigma'(0)} \right| t_c \right) \right. \\
- & i\text{Si} \left( \left( \Delta_{n_L, n_R}^{b'\sigma'(0)} + \sigma\sigma' c_{bb'} \right) t_c \right) + i\text{Si} \left( \left( \Delta_{n_L, n_R}^{b'\sigma'(0)} \right) t_c \right) \\
& \left. - (t_c \rightarrow t_c^0) \right\}. \tag{B9}
\end{aligned}$$

If  $\Delta = 0$  the replacement

$$\text{Ci} \left( \left| \Delta_{n_L, n_R}^{b'\sigma'(0)} \right| t_c^0 \right) \rightarrow \gamma + \ln \left| \Delta_{n_L, n_R}^{b'\sigma'(0)} \right| + \ln(t_c) \tag{B10}$$

has to be made. The summations over  $\sigma$  and  $\sigma'$  run over  $\pm 1$  and the parameters  $c_{b,b'}$  are given by

$$\begin{aligned}
c_{LL} &= 2E_{CL}, c_{RR} = 2E_{CR} \\
c_{MM} &= 2(E_{CL} + E_{CR} - E_{CM}) \\
c_{ML} &= c_{LM} = E_{CM} - 2E_{CL} \\
c_{LR} &= c_{RL} = E_{CM} \\
c_{MR} &= c_{RM} = 2E_{CR} - E_{CM}.
\end{aligned} \tag{B11}$$

The quantities on the right-hand sides are the charging energies  $E_{Cb}$  from Eq.(1).

<sup>1</sup> D.V. Averin and K.K. Likharev, in *Mesoscopic Phenomena in Solids*, ed. B.L. Altshuler *et al.* (Elsevier, 1991).

<sup>2</sup> *Single Charge Tunneling*, NATO ASI Series **294**, H. Grabert and M.H. Devoret, eds., (Plenum Press, 1992).

<sup>3</sup> G. Schön, Chapter 3 *Single-Electron Tunneling in Quantum Processes and Dissipation*, T. Dittrich *et al.* (Wiley-VCH Verlag).

<sup>4</sup> H. Schoeller, in “Mesoscopic Electron Transport”, eds. L.L. Sohn, L.P. Kouwenhoven, and G. Schön, NATO ASI Series E, Vol. 345 (Kluwer, 1997), p.291.

<sup>5</sup> D.V. Averin and A.A. Odintsov, Phys. Lett. A **40**, 251 (1989); D.V. Averin and Yu.V. Nazarov, Phys. Rev. Lett. **65**, 2446 (1990); in Chapter 6 in Ref. [2].

<sup>6</sup> J. König, H. Schoeller, and G. Schön, Phys. Rev. Lett. **78**, 4482 (1997); J. König, H. Schoeller, and G. Schön, Phys. Rev. B **58**, 7882 (1998).

<sup>7</sup> H. Schoeller and G. Schön, Phys. Rev. B **50**, 18436 (1994); Physica B **203**, 423 (1994).

<sup>8</sup> J. König, H. Schoeller and G. Schön, Europhys. Lett. **31**, 31 (1995); and in *Quantum Dynamics of Submicron Structures*, eds. H. A. Cerdeira *et al.*, NATO ASI Series E, Vol. 291 (Kluwer, 1995), p.221.

<sup>9</sup> P. Joyez, V. Bouchiat, D. Esteve, C. Urbina, and M.H. Devoret, Phys. Rev. Lett. **79**, 1349 (1997).

<sup>10</sup> F.R. Waugh, M.J. Berry, D.J. Mar, and R.M. Westervelt, Phys. Rev. Lett. **75**, 705 (1995); F.R. Waugh, M.J. Berry, C.H. Crouch, C. Livermore, D.J. Mar, R.M. Westervelt, K.L. Campman, and A.C. Gossard, Phys. Rev. B **53**, 1413 (1996).

<sup>11</sup> L.W. Molenkamp, Karsten Flensberg, and M. Kemerink, Phys. Rev. Lett. **75**, 4282 (1995).

<sup>12</sup> K.A. Matveev, L.I. Glazman, and H.U. Baranger, Phys. Rev. B **53**, 1034 (1996).

<sup>13</sup> K.A. Matveev, L.I. Glazman, and H.U. Baranger, Phys. Rev. B **54**, 5637 (1996).

<sup>14</sup> J.M. Golden and B.I. Halperin, Phys. Rev. B **53**, 3893 (1996); Phys. Rev. B **56**, 4716 (1997).

<sup>15</sup> J.M. Golden and B.I. Halperin Phys. Rev. B **54**, 16757 (1996).

<sup>16</sup> N. Andrei, G.T. Zimányi, and G. Schön, preprint cond-mat/9711098.

<sup>17</sup> For example, Joyez *et al.*<sup>9</sup> report to have of the order of  $10^6$  channels in the junctions for SET's in the strong tunneling regime.

<sup>18</sup> J. König, H. Schoeller, and G. Schön, Phys. Rev. Lett. **76**, 1715 (1996); J. König, J. Schmid, H. Schoeller, and G. Schön, Phys. Rev. B **54**, 16820 (1996).

<sup>19</sup> J. König and H. Schoeller, Phys. Rev. Lett. **81**, 3511 (1998).

<sup>20</sup> K.A. Matveev, Zh. Eksp. Teor. Fiz. **99**, 1598 (1991) [Sov. Phys. JETP **72**, 892 (1991)].

<sup>21</sup> The rate  $\Sigma_{\chi',\chi}^{b+}$  for processes which change the state from  $\chi'$  to  $\chi$  has the following diagrammatic representation: the rightmost tunneling line corresponds to the barrier  $b$ , and it is an outgoing (incoming) one if the rightmost vertex lies on the upper (lower) propagator. As an example, the three processes depicted in Fig.5 contribute to rates  $\Sigma_{(0,0),(1,0)}^{L+}$ ,  $\Sigma_{(1,0),(0,1)}^{R-}$ , and  $\Sigma_{(0,1),(0,1)}^{L+}$ , respectively.

<sup>22</sup> The terms  $\Delta^{(1)}(n_\sigma)$  and  $\alpha_b^{(2)}$  are the leading corrections to the bare parameters and are of the order  $O(\alpha_0)$  and  $O(\alpha_0^2)$ , respectively. (Note:  $\alpha_0^b$  is of 1st and its correction of 2nd order, while  $\Delta^{(0)}$  is of 0th and its correction of 1st order.)

<sup>23</sup> The set of states required for the completeness of the theory in second order can be found as follows: take the charge states reachable via sequential tunneling and include all states which may be reached from these via an arbitrary process of the 1st order – these states are virtually occupied during tunneling processes.